

## Supporting information

# Efficient CO<sub>2</sub> electroreduction to formate by Bi-Pb bimetallic catalysts with 2D vertically nanosheets

Chongyang Jiang,<sup>a</sup> Shaojuan Zeng,<sup>\*a</sup> Jiaqi Feng,<sup>b</sup> Guilin Li,<sup>a</sup> Bin Hai,<sup>c</sup> Kuilin Peng,<sup>a</sup>

Xiangping Zhang<sup>\*a</sup>

<sup>a</sup> Beijing Key Laboratory of Ionic Liquids Clean Process, State Key Laboratory of Multiphase Complex Systems, CAS Key Laboratory of Green Process and Engineering, Institute of Process Engineering, Chinese Academy of Sciences, Beijing, 100190, China

<sup>b</sup> Beijing National Laboratory for Molecular Sciences, Key Laboratory of Colloid and Interface and Thermodynamics, Institute of Chemistry, Chinese Academy of Sciences, Beijing, 100190, China

<sup>c</sup> College of Chemistry and Chemical Engineering, Henan University, Kaifeng, 475000, China

\*E-mail address: [sjzeng@ipe.ac.cn](mailto:sjzeng@ipe.ac.cn) (S. Zeng); [xpzhang@ipe.ac.cn](mailto:xpzhang@ipe.ac.cn) (X. Zhang)

## **Supplementary Notes**

### **Experimental section**

Carbon paper (CP, 99.8%) with 1.5 mm thickness was purchased from Shanghai Hesen Co., Ltd. Hydrochloric acid (HCl, 36.5%) and sulfuric acid (H<sub>2</sub>SO<sub>4</sub>, 98%) were obtained from Beijing Chemical Works. Lead acetate (Pb(CH<sub>3</sub>COO)<sub>2</sub>, 99.8%), sodium fluoride (NaF, 99.8%), potassium bicarbonate (KHCO<sub>3</sub>, 99.8%), acetonitrile (AcN, 99.8%), bismuth nitrate (Bi(NO<sub>3</sub>)<sub>3</sub>, 99.8%) and acetone (CH<sub>3</sub>COCH<sub>3</sub>) were purchased from Shanghai Macklin Biochemical Co., Ltd. The 1-butyl-3-methylimidazolium tetrafluoroborate ionic liquid ([Bmim][BF<sub>4</sub>], 98%) was purchased from Shanghai Chengjie Co., Ltd.

### **Characterizations**

Scanning electron microscope (SEM, Hitachi SU8020) and Transmission electron microscope (TEM, JEOL JEM-2100 system) were employed to observe the morphologies of the catalysts. X-ray diffraction (XRD, Rigaku Smartlab diffractometer) and X-ray photoelectron spectroscopy (XPS, Thermo Fisher Scientific ESCALAB 250Xi) were used to confirm the crystal structures and elemental compositions, respectively. Inductively coupled plasma spectrometry (ICP) was carried on an ICPE-9000 to determine the metal content.

### **Product analysis**

The main products of CO<sub>2</sub> electroreduction are formate, CO, and H<sub>2</sub>, respectively. Gas products were quantified by gas chromatography (GC, Agilent 7890A GC) with a thermal conductivity detector (TCD) and a flame ionization detector (FID). N<sub>2</sub> was

used as the carrier gas. The gases from the outlet of the cathodic compartment were collected by a gas bag, and then injected into the GC. Every gas sample was measured three times.

The concentration of liquid products was detected using a 600 MHz  $^1\text{H}$  liquid NMR spectrometer (Bruker Advance). Phenol was used as an internal reference for the liquid products. The standard solution consisted of  $0.5 \times 10^{-3}$  M phenol and DMSO. Typically, NMR samples were prepared by mixing 300  $\mu\text{L}$  of the product-containing electrolyte and 200  $\mu\text{L}$  standard solution. Two electrons are needed to produce one CO, H<sub>2</sub> and formate molecule, so the FE of the CO<sub>2</sub> electroreduction products can be calculated as follows (Equation (1)):

$$\text{FE} = 2Fn/Q \quad (1)$$

Where  $F$  is the Faraday constant, 96485 C mol<sup>-1</sup>;  $n$  is the molar amount of product, mol; and  $Q$  is the charge recorded by electrochemical workstation, C.

The formula for calculating the production rate of formate was as follow (Equation (2)).

$$\text{The production of formate} = \frac{n_{\text{formate}}}{t \times S} \quad (2)$$

Where  $n_{\text{formate}}$  is the molar amount of formate (mol), quantified by NMR;  $t$  is the electroreduction reaction time (h);  $S$  is the geometric area of the catalyst.

## DFT calculations

In order to investigate the origin of the high performance of Bi-Pb bimetallic catalysts, theoretical calculations were carried out using periodic DFT implemented in the Vienna Ab initio Simulation Package (VASP 5.4.4). The projector-augmented

method was applied to solve the ion-electron interaction in a periodic system. The generalized gradient approximation with Perdew-Burke-Ernzerh of functionals was used to treat the exchange-correlation interactions in the Kohn-Sham equations. Spin-polarized calculations were carried out with an energy cutoff for the plane waves of 520 eV. The convergence criteria for optimization of the atomic structure were set at  $1 \times 10^{-5}$  eV and a Hellmann-Feynman force of 0.02 eV Å<sup>-1</sup>. A Monkhorst-Pack *k*-point mesh of  $5 \times 5 \times 1$  *k*-points was employed. The Pb(111) surface with four atomic layers and  $5 \times 5$  unit cells was used as the model system. In order to simulate the role of Bi on this bimetallic catalyst, a Bi-Pb(111) surface was built by decorating Bi atom onto the surface of pure Pb(111) surface. A vacuum layer of 15 Å was added to separate neighbouring slabs to avoid possible interaction.

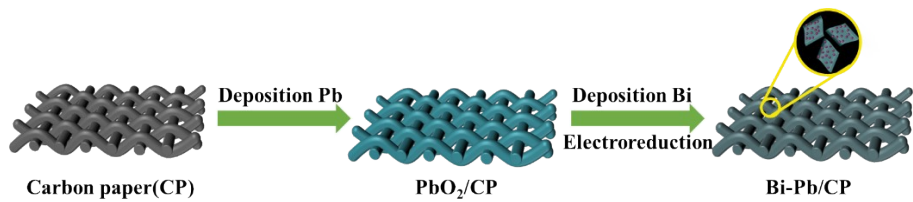


Fig. S1. The schematic of the synthesis process for the Bi-Pb bimetallic catalyst

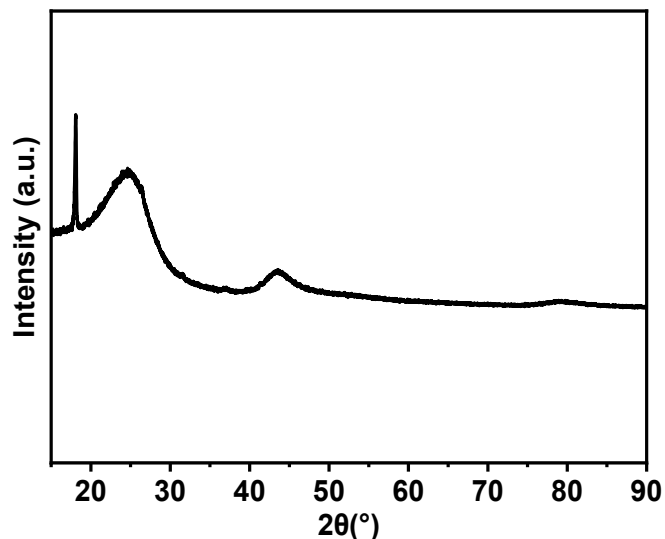


Fig. S2. XRD pattern of pure carbon paper

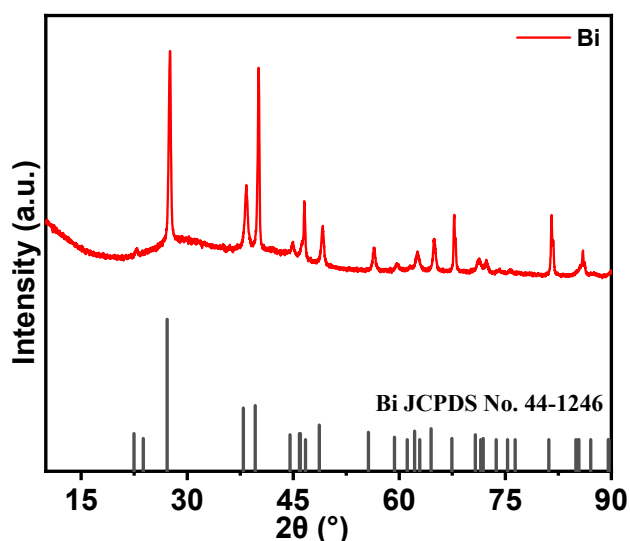


Fig. S3. XRD pattern of Bi/CP electrode

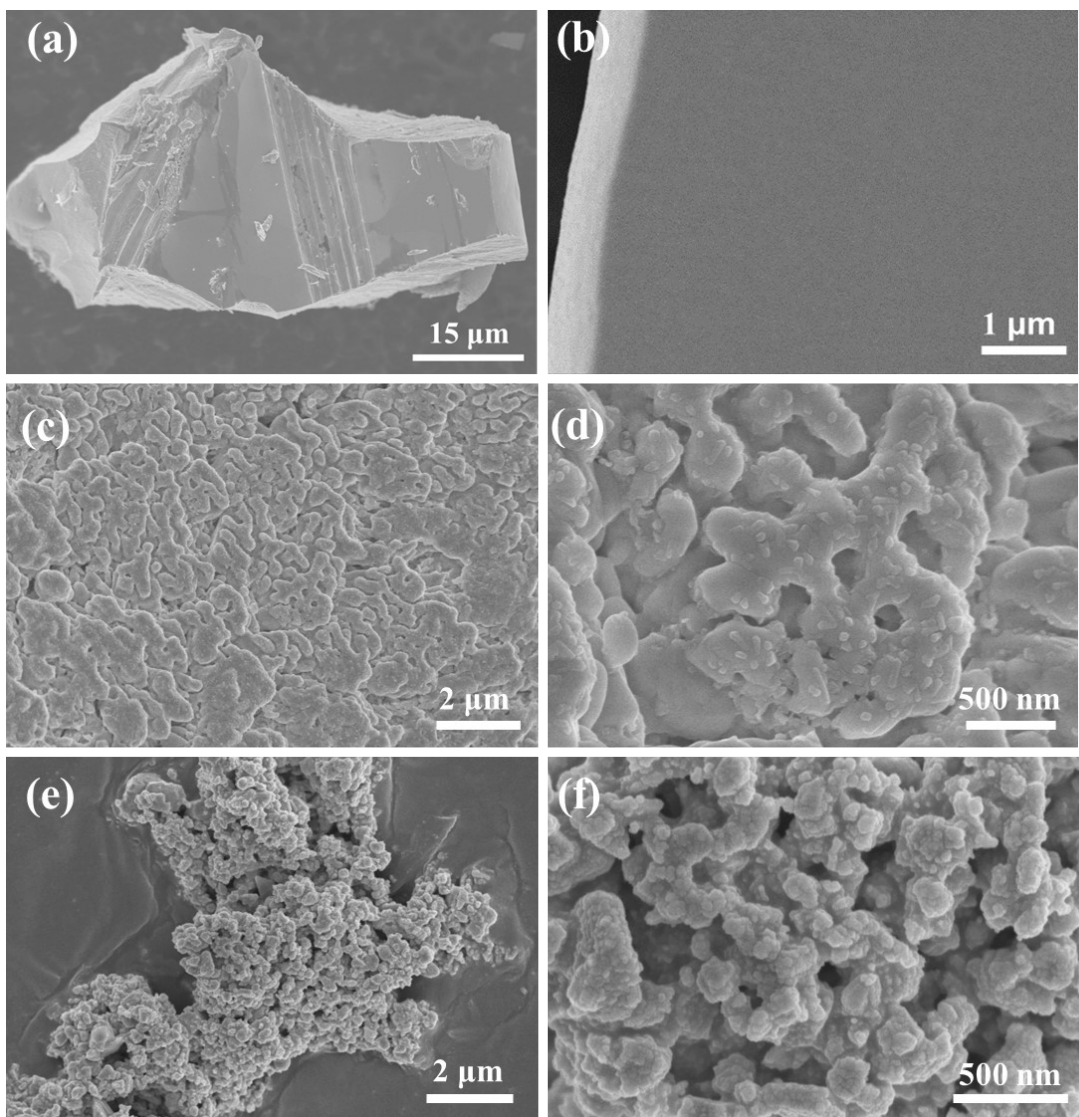


Fig. S4. SEM images of PbO<sub>2</sub>/CP (a, b), Bi-PbCl<sub>2</sub>/CP (c, d), and Bi/CP (e-f)

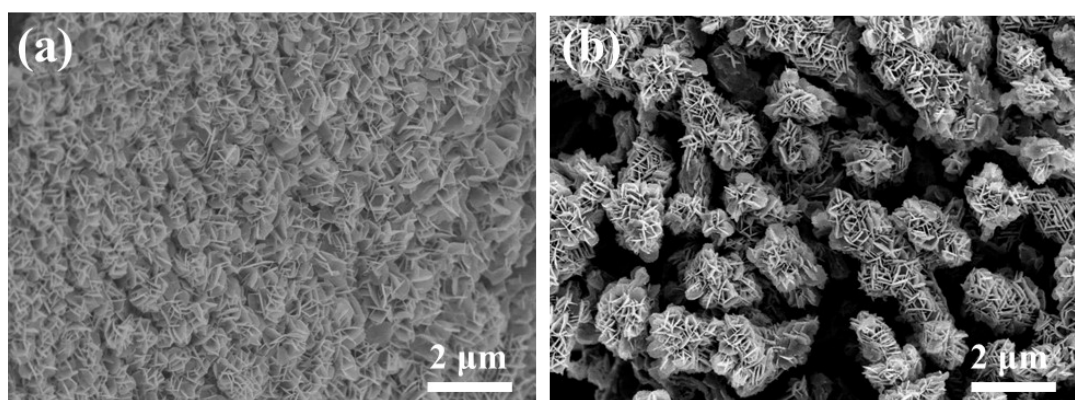


Fig. S5. SEM images of PbO<sub>2</sub>/CP (a) and Bi-PbCl<sub>2</sub>/CP (b) after electroreduction

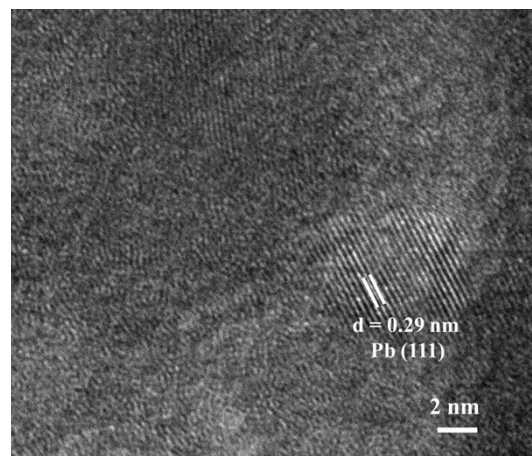


Fig. S6. TEM image of  $\text{PbO}_2/\text{CP}$  after electroreduction

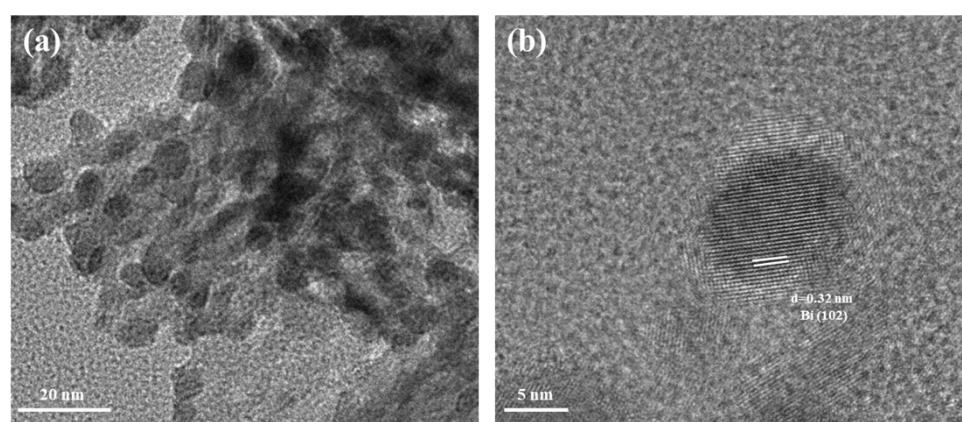


Fig. S7. TEM images of  $\text{Bi}/\text{CP}$  catalyst

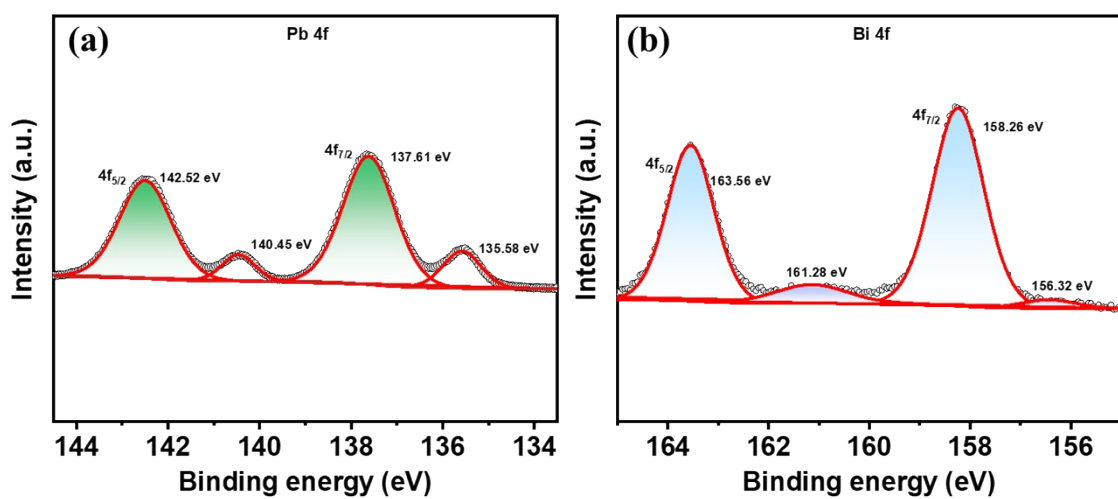


Fig. S8.  $\text{Pb} 4f$  spectra of  $\text{PbO}_2/\text{CP}$  (a) after electroreduction and  $\text{Bi} 4f$  spectra of  $\text{Bi}/\text{CP}$  (b)

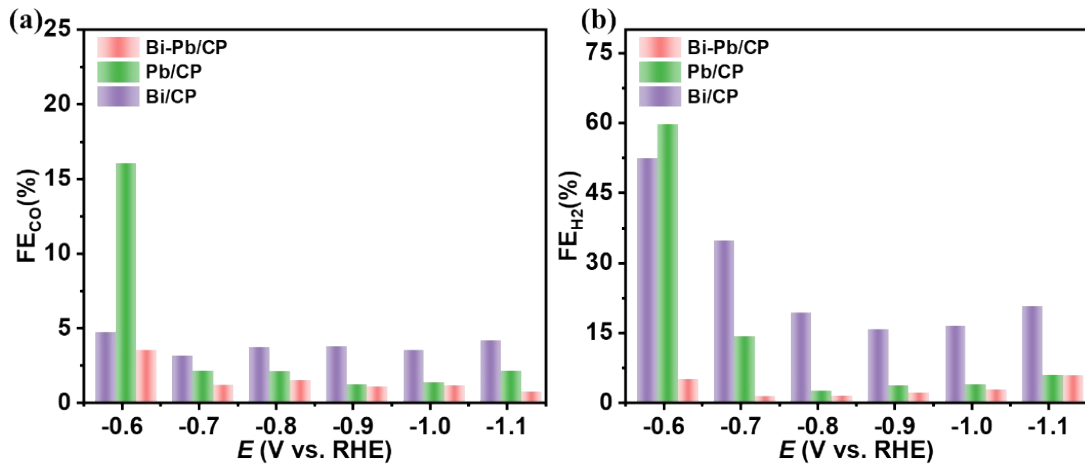


Fig. S9. The FE of CO (a) and H<sub>2</sub> (b) at various applied potentials for Pb/CP, Bi/CP, and Bi-Pb/CP in 0.5 M KHCO<sub>3</sub> solution

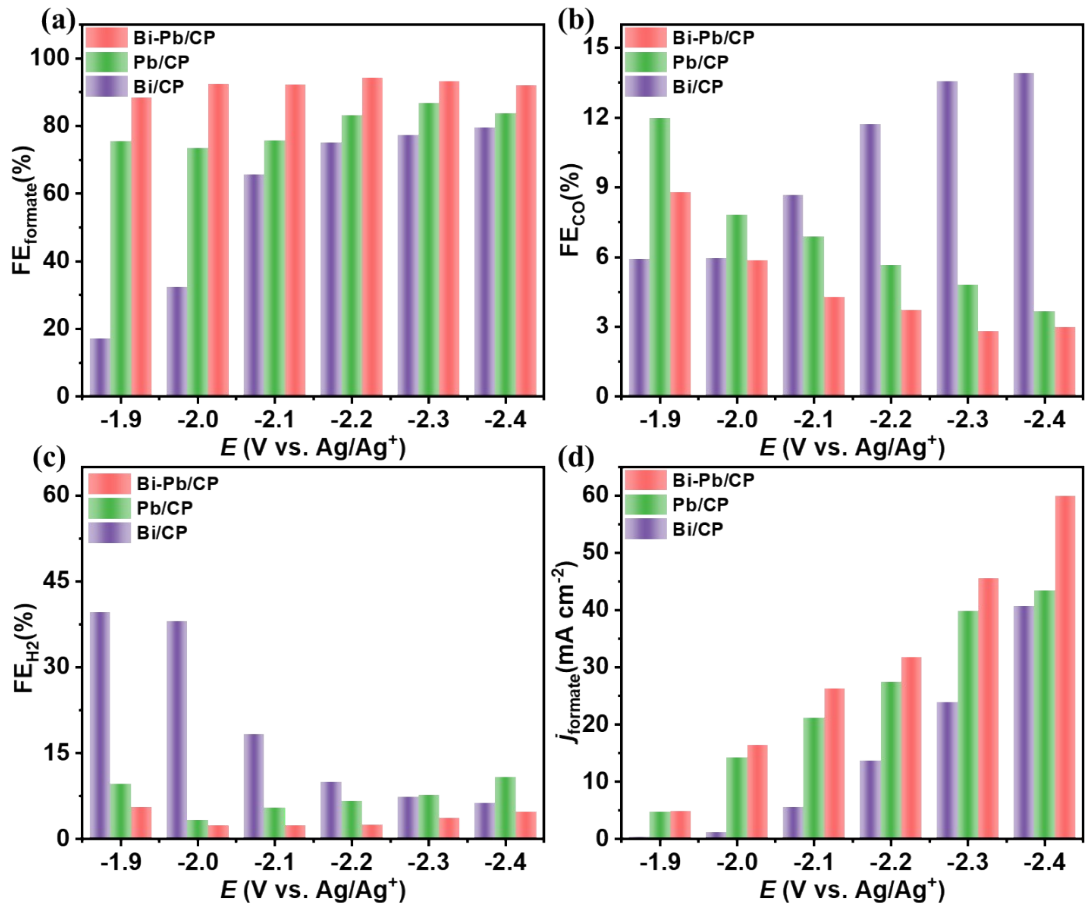


Fig. S10 The FE of formate (a), CO (b) and H<sub>2</sub> (c) at various applied potentials for Pb/CP, Bi/CP, and Bi-Pb/CP in 30 wt%[Bmim][BF<sub>4</sub>]/AcN-H<sub>2</sub>O (5 wt%) IL electrolyte

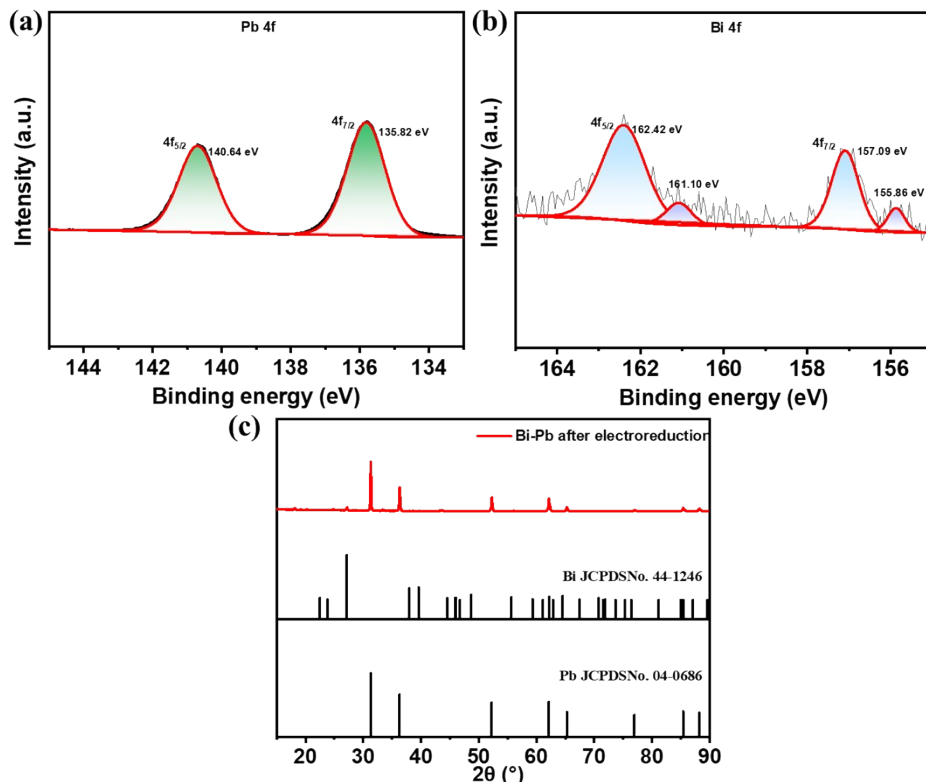


Fig. S11. XPS spectra of Pb 4f (a) and Bi 4f (b) and XRD pattern (c) of Bi-Pb/CP after 10 h electrolysis

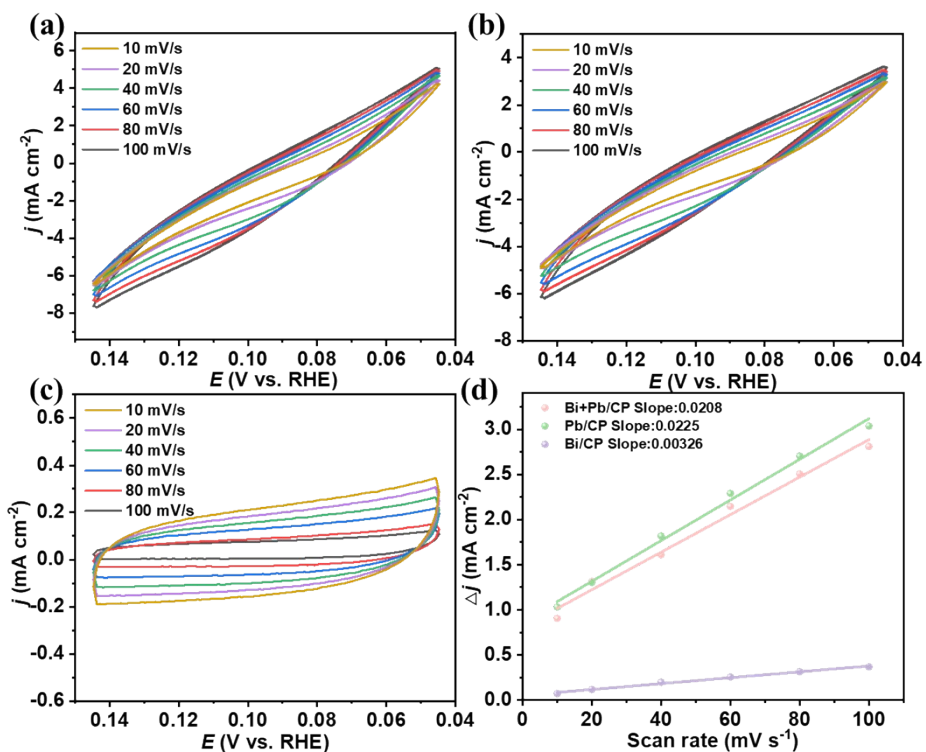


Fig. S12. Cyclic voltammograms at the range of -0.55 to -0.65 V with different scan rates (10, 20, 40, 60, 80, 100 mV s<sup>-1</sup>) for Pb/CP (a), Bi-Pb/CP (b) and Bi/CP (c); Charging current density differences plotted against scan rate (d)

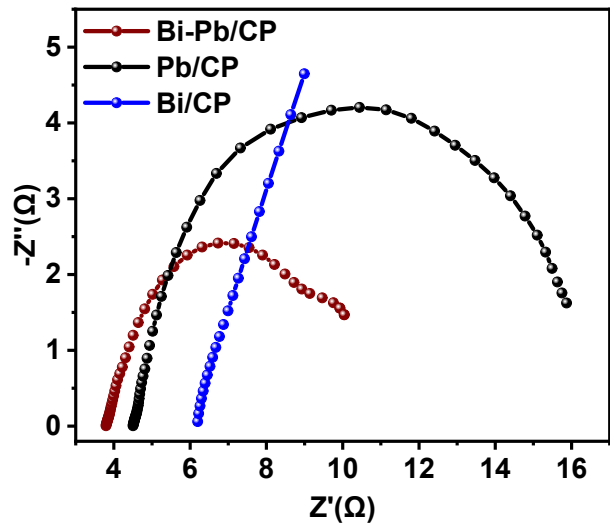


Fig. S13. Nyquist plots for Pb/CP, Bi/CP and Bi-Pb/CP

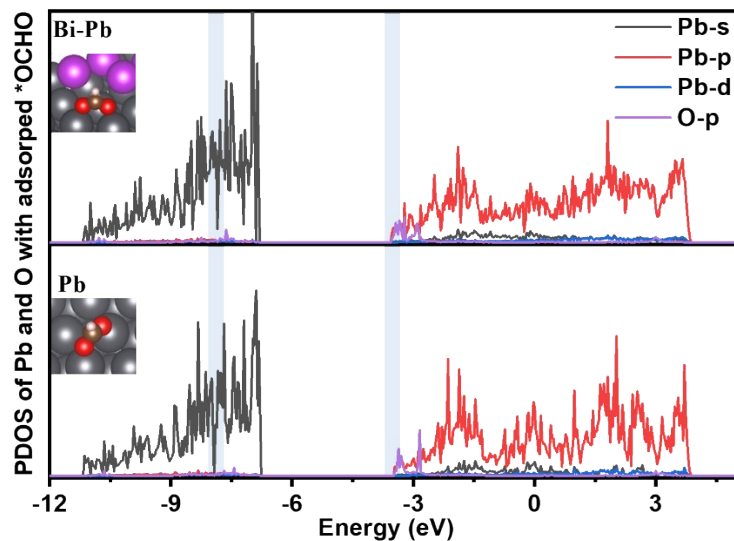


Fig. S14. The DOS of Pb atom and O atom on Bi-Pb(111) and Pb(111) surfaces with adsorbed \*OCHO

Table S1. Current density and FE of formate in CO<sub>2</sub> electrochemical reduction using various electrodes and catholytes in H-type cell

Catalysts	Electrolyte	Potential (V)	FE <sub>formate</sub> (%)	$j_{\text{formate}}(\text{mA cm}^{-2})$	Formate formation rate ( $\mu\text{mol h}^{-1} \text{cm}^{-2}$ )	Ref.
Bi flake	0.1 M KHCO <sub>3</sub>	-0.6 vs RHE	99	4	74.6	1
	0.5 M KHCO <sub>3</sub>	-1.1 vs RHE	90	45	839.4	2
Bi-MOF	0.1 M KHCO <sub>3</sub>	-0.9 vs RHE	92	4	74.6	3
	0.1 M KHCO <sub>3</sub>	-0.8 vs RHE	97	3.8	70.9	4
Bi nanosheet with vacancies	0.5 M NaHCO <sub>3</sub>	-1.0 vs RHE	97	25	466.3	5
Bi nanotubes	0.5 M KHCO <sub>3</sub>	-0.8 vs RHE	93	30	599.6	6
Bi nanosheet	0.5 M NaHCO <sub>3</sub>	-1.8 vs SCE	96.4	15.2	283.5	7
S-Bi/Ag	0.5 M NaHCO <sub>3</sub>	-1.0 vs RHE	94.7	28.1	561.6	8
Bi <sub>2</sub> O <sub>3</sub> -NGQDs	0.5 M KHCO <sub>3</sub>	-0.87 vs RHE	98	16.6	309.6	9
Helical Bi <sub>2</sub> O <sub>3</sub> microfibers	0.1 M KHCO <sub>3</sub>	-1.2 vs RHE	90	13	242.4	10
Eutectic Bi-Sn	0.1 M KHCO <sub>3</sub>	-1.1 vs RHE	78	10.7	199.6	11
Bi@Bi <sub>2</sub> O <sub>2</sub> CO <sub>3</sub>	0.5 M KHCO <sub>3</sub>	-0.8 vs RHE	97	38	708.8	12
Nafion/Bi NSs@Cu foam	0.5 M KHCO <sub>3</sub>	-0.97 vs RHE	97.3	36	671.5	13
Pd-Bi nanosheet	0.5 M KHCO <sub>3</sub>	-1.0 vs RHE	91.9	25	466.3	14
CuBi	0.5 M KHCO <sub>3</sub>	-1.2 vs RHE	90.8	33	615.5	15
Pb QDDCs	0.5 M KHCO <sub>3</sub>	-0.2 vs RHE	95	16	298.4	16
Pb NP/MWCNT	0.5 M KHCO <sub>3</sub>	-1.8 vs Ag/AgCl	70	30	559.6	17
Sulfide-derived Pb	0.1 M KHCO <sub>3</sub>	-1.08 vs RHE	88	12	223.8	18
Bi@np-Cu	0.5 M KHCO <sub>3</sub>	-0.97 vs RHE	97.7	82	1529.5	19

Ag-loaded Bi <sub>2</sub> O <sub>2</sub> CO <sub>3</sub>	0.5 M KHCO <sub>3</sub>	-1.1 vs RHE	95.8	15.3	285.4	20
Bi <sub>2</sub> O <sub>2</sub> CO <sub>2</sub> modified with iodine and pyrenyl-graphdiyne	0.5 M KSO <sub>4</sub> (pH: 3.5)	-1.4 vs RHE	94.84	~60	-	21
CuBi <sub>3</sub>	0.1 M KHCO <sub>3</sub>	-1.3 vs RHE	98.3	21.2	396.1	22
Ce leaching-derived Bi nanosheets	0.5 M KHCO <sub>3</sub>	-1.4 vs RHE	95	46.4	865.5	23
Bi-MOFs	0.1 M KHCO <sub>3</sub>	-1.1 vs RHE	90.4	20.8	-	24
3D bi-continuous nanoporous bismuth	0.1 M KHCO <sub>3</sub>	-0.956 vs RHE	92.6	5	93.2	26
dendritic Bi film	0.1 M KHCO <sub>3</sub>	-0.90 vs RHE	~80	8.6	160.4	27
2D Bi <sub>2</sub> S <sub>3</sub> NSS	0.5 M KHCO <sub>3</sub>	-0.93 vs RHE	~95	~30	559.6	28
Sb <sub>2.5</sub> /Bi@C	0.5 M KHCO <sub>3</sub>	-1.4 vs Ag/AgCl	94.8	~5	93.3	29
5% Bi-InOCl	0.5 M NaHCO <sub>3</sub>	-0.9 vs RHE	89.9	14.89	277.7	30
Bi <sub>2</sub> O <sub>2</sub> CO <sub>3</sub> ultrathin nanosheets	0.5 M NaHCO <sub>3</sub>	-0.9 vs RHE	96	25	466.3	31
Cu-doped Bi catalyst	0.1 M KHCO <sub>3</sub>	-1.1 vs RHE	94	20	373.3	32
Bi-Cr <sub>2</sub> O <sub>3</sub> nano-dendrites	1.0 M KHCO <sub>3</sub>	-1.1 vs RHE	93.3	40.7	759.2	33
Bi-Pb	0.5 M KHCO <sub>3</sub>	-1.1 vs RHE	93.0	53.1	990.5	This work

## Reference

- 1 S. Kim, W. J. Dong, S. Gim, W. Sohn, J. Y. Park, C. J. Yoo, H. W. Jang and J.-L. Lee, *Nano Energy*, 2017, **39**, 44-52.
- 2 S.-Q. Liu, M.-R. Gao, R.-F. Feng, L. Gong, H. Zeng and J.-L. Luo, *ACS Catal.*, 2021, **11**, 7604-7612.
- 3 F. Li, G. H. Gu, C. Choi, P. Kolla, S. Hong, T.-S. Wu, Y.-L. Soo, J. Masa, S. Mukerjee, Y. Jung, J. Qiu and Z. Sun, *Appl. Catal. B*, 2020, **277**, 119241.
- 4 M. Zhao, Y. Gu, W. Gao, P. Cui, H. Tang, X. Wei, H. Zhu, G. Li, S. Yan, X. Zhang and Z. Zou, *Appl. Catal. B*, 2020, **266**.
- 5 K. Fan, Y. Jia, Y. Ji, P. Kuang, B. Zhu, X. Liu and J. Yu, *ACS Catal.*, 2019, **10**, 358-364.
- 6 J. Fan, X. Zhao, X. Mao, J. Xu, N. Han, H. Yang, B. Pan, Y. Li, L. Wang and Y. Li, *Adv. Mater.*, 2021, **33**.
- 7 H. Zhong, Y. Qiu, T. Zhang, X. Li, H. Zhang and X. Chen, *J. Mater. Chem. A*, 2016, **4**, 13746-13753.
- 8 J. Liu, Y. Li, Y. Wang, C. Xiao, M. Liu, X. Zhou, H. Jiang and C. Li, *Nano Research*, 2021, **15**, 1409-1414.

- 9 Z. Chen, K. Mou, X. Wang and L. Liu, *Angew. Chem. Int. Ed.*, 2018, **57**, 12790-12794.
- 10 H. Ning, Y. Wang, X. Fei, X. Wang, X. Jin, Y. Zou, C. Ma, Z. Jiao, Y. Zhao and M. Wu, *ChemSusChem*, 2023, **16**, e202201810.
- 11 J. Tang, R. Daiyan, M. B. Ghasemian, S. A. Idrus-Saidi, A. Zavabeti, T. Daeneke, J. Yang, P. Koshy, S. Cheong, R. D. Tilley, R. B. Kaner, R. Amal and K. Kalantar-Zadeh, *Nat. Commun.*, 2019, **10**, 4645.
- 12 X.-D. Liang, Q.-Z. Zheng, N. Wei, Y.-Y. Lou, S.-N. Hu, K.-M. Zhao, H.-G. Liao, N. Tian, Z.-Y. Zhou and S.-G. Sun, *Nano Energy*, 2023, **114**.
- 13 S. Chang, Y. Xuan, J. Duan and K. Zhang, *Appl. Catal. B*, 2022, **306**.
- 14 L. Xie, X. Liu, F. Huang, J. Liang, J. Liu, T. Wang, L. Yang, R. Cao and Q. Li, *Chinese J. Catal.*, 2022, **43**, 1680-1686.
- 15 M. Y. Zu, L. Zhang, C. Wang, L. R. Zheng and H. G. Yang, *J. Mater. Chem. A*, 2018, **6**, 16804-16809.
- 16 M. Liu, M. Liu, X. Wang, S. M. Kozlov, Z. Cao, P. De Luna, H. Li, X. Qiu, K. Liu, J. Hu, C. Jia, P. Wang, H. Zhou, J. He, M. Zhong, X. Lan, Y. Zhou, Z. Wang, J. Li, A. Seifitokaldani, C. T. Dinh, H. Liang, C. Zou, D. Zhang, Y. Yang, T.-S. Chan, Y. Han, L. Cavallo, T.-K. Sham, B.-J. Hwang and E. H. Sargent, *Joule*, 2019, **3**, 1703-1718.
- 17 Y. Xing, M. Cui, P. Fan, J. Ren, C. Zhang, N. Li, X. Wen and X. Ji, *Mater. Chem. Phys.*, 2019, **237**, 121826.
- 18 J. E. Pander, J. W. J. Lum and B. S. Yeo, *J. Mater. Chem. A*, 2019, **7**, 4093-4101.
- 19 Q. Zhao, J. Wang, Y. Zhuang, L. Gong, W. Zhang, W. Fan, Z. Lu, Y. Zhang, T. Fujita, P. Zhang and Q. Xue, *Sci. China Mater.*, 2024, **67**, 796-803.
- 20 W. Zheng, C. Wang, J. Chen, S. Chen, Z. Lin, M. Huang, H. Huang, Y. Qu, P. Wang, L. Hu and Q. Chen, *Dalton Trans.*, 2024, **53**, 4617- 4623.
- 21 M. Zhang, J. Wang, X. Rong, X.-L. Lu and T.-B. Lu, *Nano Research*, 2023, **17**, 2381-2387.
- 22 Y. Fu, K. Leng, H. Zhuo, W. Liu, L. Liu, G. Zhou and J. Tang, *J. CO<sub>2</sub> Util.*, 2023, **70**, 102456.
- 23 J. Zhu, Y. Tong, H. B. Xu, X. Ren, X. Peng and P. Chen, *Acs Sustain. Chem. Eng.*, 2023, **12**, 938-946.
- 24 L. Li, X. Kang, M. He, A. Sheveleva, K. Hu, S. Xu, Y. Zhou, J. Chen, S. Sapchenko, G. Whitehead, I. J. Vitorica-Yrezabal, L. Lopez-Odriozola, L. S. Natrajan, E. J. L. McInnes, M. Schröder, S. Yang and F. Tuna, *J. Mater. Chem. A*, 2022, **10**, 17801-17807.
- 25 C. Lin, Y. Liu, X. Kong, Z. Geng and J. Zeng, *Nano Research*, 2022, **15**, 10078-10083.
- 26 W. Lai, Y. Liu, M. Zeng, D. Han, M. Xiao, S. Wang, S. Ren and Y. Meng, *Nanomaterials*, 2023, **13**, 1767.
- 27 F. Lhostis, N. H. Tran, G. Rousse, S. Zanna, N. Menguy and M. Fontecave, *ChemElectroChem*, 2024, DOI: 10.1002/celc.202300799, e202300799.
- 28 Y. Li, J. Chen, S. Chen, T. Lu, X. Liao, T. Zhao, F. Cheng and H. Wang, *Appl. Catal. B*, 2024, **349**, 123874.
- 29 S. Ma, K. Wu, S. Fan, Y. Li, Q. Xie, J. Ma and L. Yang, *Sep. Purif. Technol.*, 2024, **339**, 126520.
- 30 Y. Jia, H. Yang, R. Chen, Y. Zhang, F. Gao, C. Nan, J. Yang and X. Gao, *J. Alloys Compd.*, 2024, **987**, 174220.
- 31 Q. Huang, X. Sha, R. Yang, H. Li and J. Peng, *ACS Appl. Mater. Inter.*, 2024, **16**, 13882-13892.
- 32 Y. Wei, X. Xu, D. Shi, Y. Jiang, C. Zheng, L. Tan, Z. Liu, S. Zhong and Y. Yu, *Small*, 2024, DOI: 10.1002/smll.202401017, e2401017.

33 F. Kong, C. Wen, L. Kang, P. Gao, L. Dong, B. Li, H. He, M. Fan and Z. Chen, *Molecular Catalysis*, 2024, **559**, 114118.